iScience

CellPress
OPEN ACCESS

Article

Binder assisted graphene derivatives as lubricants in copper: Improved tribological performance for industrial application

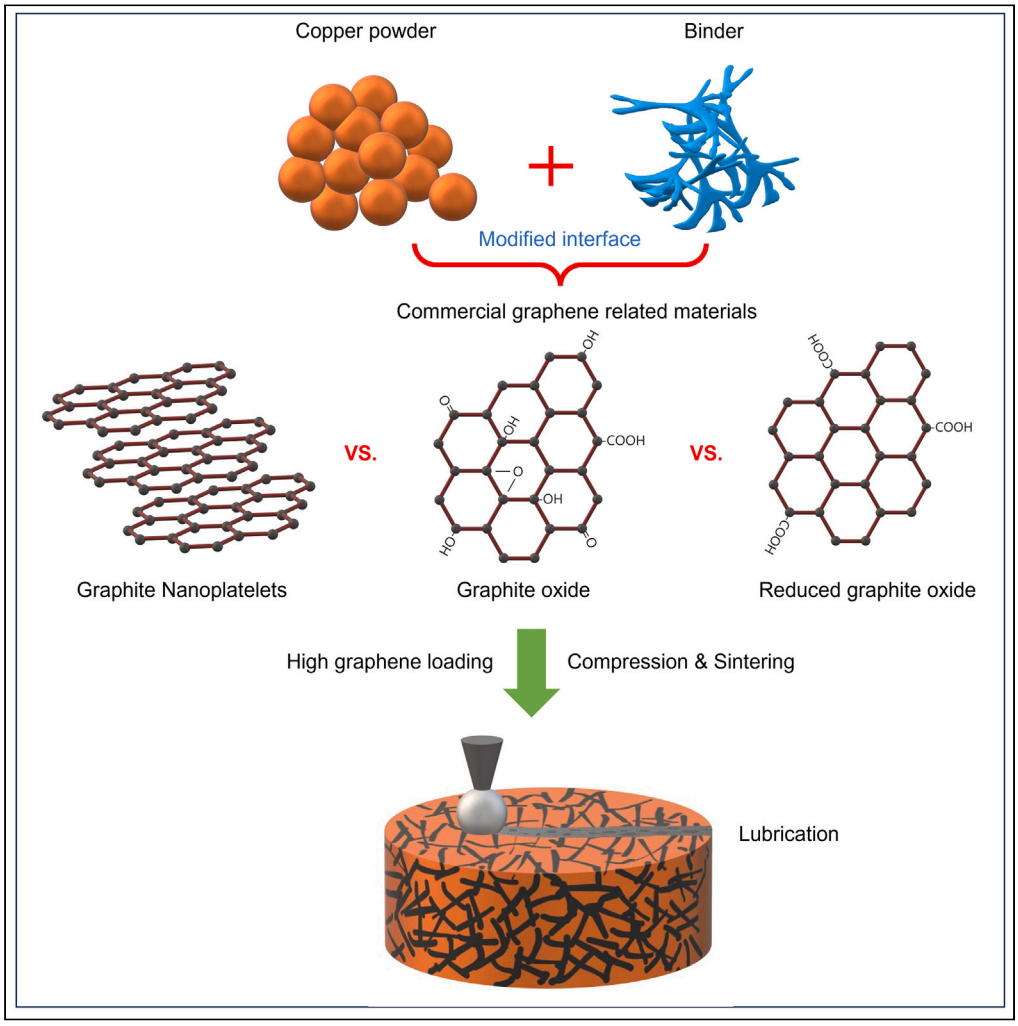

Changjie Huang, Su Zhao, Ruiqi Chen, ..., Mamoun Taher, Vincenzo Palermo, Jinhua Sun

jinhua@chalmers.se

Highlights

Commercial graphene derivatives as lubricant in Cu were systematically investigated

The interface between graphene and Cu particles was improved using sustainable binders

High graphene loading was achieved and uniformly distributed in Cu matrix

The most favorable graphene derivatives for tribology application were identified

Huang et al., iScience 27, 109429
April 19, 2024
https://doi.org/10.1016/j.isci.2024.109429

iScience

CellPress
OPEN ACCESS

Article

Binder assisted graphene derivatives as lubricants in copper: Improved tribological performance for industrial application

Changjie Huang,[1] Su Zhao,[2] Ruiqi Chen,[1] Erik Johansson,[2] Muhammad Aqeel,[1] Uta Klement,[1] Anna M. Andersson,[2] Mamoun Taher,[3] Vincenzo Palermo,[1,4] and Jinhua Sun[1,5,*]

SUMMARY

Originally derived from graphite, high-quality single-layer graphene is an excellent anti-wear and -friction additive in metal matrix. Here, the tribological performance of 3 different commercialized graphene derivatives (e.g., graphene oxide [GO], reduced graphene oxide [RGO], and graphene nanoplatelet [GNP]) as additives in a Cu matrix, were investigated from an industrial perspective. To increase the interaction of graphene derivatives with Cu particles, and addressing the aggregation problem of the graphene derivatives, different binders (polyvinyl alcohol [PVA] and cellulose nanocrystals [CNC]) were introduced into the system. Benefiting from such a strategy, a uniform distribution of the graphene derivatives in Cu matrix was achieved with graphene loading up to 5 wt %. After high-temperature sintering, the graphene is preserved and well distributed in the Cu matrix. It was found that the GNP-containing sample shows the most stable friction coefficient behavior. However, GO and RGO also improve the tribological performance of Cu under different circumstances.

INTRODUCTION

Our daily life relies on friction force, from taking a walk to accelerating vehicles. However, the modern society is also hampered by friction forces, as various forms of friction cause up to 50% energy loss, which manifests itself as wear and tear.[1] Lubrication is the solution to reduce the friction and wear applied in industrial and household products. Liquid-based lubrication (e.g., oil and grease), the most popular industrial method to reduce friction and wear, offers low requirements for the friction body.[2,3] However, their implementation could be limited by complex application designs and the intrinsic properties such as oxidation stability, viscosity, thermal stability, volatility, and flammability. In addition, the maintenance of liquid-based lubricants can result in high costs and interruption of the working machine. Solid lubrication, however, is more stable for those types of applications and can be used in a harsh environment. It has been reported that micro and nano-sized particles (e.g., Al_2O_3) could provide highly effective lubrication properties.[4] Graphite is one of the commonly used solid lubricant additives, with a low price. However, it cannot work properly in a dry environment.[5] Graphene, a single layer of carbon atoms in a hexagonal pattern (one graphite layer), shows surprisingly good tribological performance even under harsh conditions because of its easy shear capability on its densely packed and atomically smooth surface.[6] In addition, due to its unique structure and extraordinary properties, graphene as additives can further improve the performance of composite materials in terms of, for example, mechanical properties, tensile strength, thermal conductivity, electric conductivity, and anticorrosion properties.[5,7]

Usually, those extraordinary properties were demonstrated for single-layer graphene derived from exfoliated graphite.[8] For practical applications at industrial scale, the availability of large-scale single-layer graphene needs to be considered. In this regard, other graphene derivatives, for example graphene oxide (GO), reduced graphene oxide (RGO), and graphene nanoplatelet (GNP) are more appropriate choices considering that they are commercially available at relatively low prices, and at mass-production capacity.[9] Different graphene derivatives have different properties, structures, and surface chemistries. For example, GO has more oxygen containing functional groups than RGO and GNP, and GNP provides a higher shearing ability than GO.[10] Therefore, the tribological performance of different graphene derivatives in regard to their properties and structures needs to be investigated in order to identify suitable additive materials in composites aimed for tribological applications.

For graphene-enhanced metal matrix composites, aggregation of graphene is a big issue, regardless of which graphene derivative is used.[11] This holds true especially for Cu-graphene composites, where the issues are caused by the weak binding energy between graphene

[1]Department of Industrial and Materials Science, Chalmers University of Technology, 41296 Göteborg, Sweden
[2]ABB AB, Corporate Research, 721 78 Västerås, Sweden
[3]Graphmatech AB, Mältargatan 17, 753 18 Uppsala, Sweden
[4]Institute of Organic Synthesis and Photoreactivity (ISOF), National Research Council of Italy (CNR), Via P. Gobetti 101, 40129 Bologna, Italy
[5]Lead contact
*Correspondence: jinhua@chalmers.se
https://doi.org/10.1016/j.isci.2024.109429

and Cu[12] and also the agglomeration of graphene due to the strong van der Waals attraction, large surface areas and π–π interaction.[13,14] We recently reported a surface modification strategy to controllably coat GO on the surface of Cu particles for anticorrosion application.[15] Simple mechanical mixing is not enough to achieve uniform distribution because of the poor interaction.[16,17]

A binder is usually introduced as an additional component to bind together two or more materials in the mixtures. For example, organic binder poly (vinylidene fluoride) (PVDF) is commonly used as binder for the formation of cathode electrode film in battery industry.[18] Apart from PVDF, water-soluble binders are highly in demand in industry because of its sustainable and economically viable features. Polyvinyl alcohol (PVA) is a typical water-soluble binder with hydroxyl groups that provide the hydrogen bond that increases the interaction between graphene and other compounds.[19] It has been demonstrated that by using PVA as a binder, carbon nanotube could attach better to aluminum particles, achieving higher homogeneity.[20,21] However, the binding effect of PVA and other water-soluble binder materials on graphene- and Cu-powder mixtures was barely investigated. A systematic investigation would here be interesting to understand the role of water-soluble binders on the interaction of different graphene derivatives in a Cu matrix, and on the tribological behavior of such composites.

Here, the tribological performance of three different graphene derivatives, GNP, GO, and RGO, was systematically investigated as lubricant additives in a Cu matrix. To prevent the agglomeration of graphene derivatives and increase their uniformity in Cu matrix, two water soluble binders were introduced with the aim to increase the interaction between graphene derivatives and Cu matrix. In the presence of optimized amount of binder, all three graphene derivatives are uniformly distributed in the Cu matrix even under a simple mixing procedure with high graphene loading up to 5 wt %. After high-temperature sintering, the graphene was preserved and well distributed in the Cu matrix, as verified by scanning electron microscopy (SEM), energy dispersive spectroscopy (EDS), Raman mapping. The tribological performance of three different graphene derivatives as additives in Cu was systematically investigated. Although the GO with smaller particle size shows better homogeneity in Cu matrix than RGO and GNP, the GNP containing sample shows the lowest and most stable friction coefficient. However, the GO and RGO can also improve the tribological performance of Cu. The wear tracks of GNP containing Cu shows the most uniform morphology and nanostructure, which helps to understand the role of GNP in reducing the friction of Cu.

RESULT AND DISCUSSION

The morphology and nanostructure of the commercial GNP, GO, and RGO materials (graphene-related materials [GRM]) were examined by SEM (Figures 1A–1C). The GNP flakes with large lateral size are composed by multilayer graphene (Figure 1A). Single layer graphene can be also observed, but most are relatively thick graphite nanoplates in a broad range of thicknesses, from less than 1 nm to tens of nanometers. The GO, on the other hand, is composed of completely exfoliated nanosheets, mainly of single-layer structure (Figure 1B), as evidenced by the presence of the typical feature of graphene wrinkles. Different from the GO, the RGO sample contains large particles with a lateral size about tens of micrometers, mainly due to the aggregation (Figure 1C). The chemical composition of the GO, RGO, and GNP was investigated by the XPS and TGA (Figures S2 and S3; Table S1). As expected, the GO contains more oxygen containing functional groups than RGO and GNP.[22]

SEM images of the pressed GRM/Cu composite samples with 3 wt % graphene loading are shown in Figures 1D–1F and S5. The 3 wt % graphene was first investigated with the aim to reach a certain amount of loading of graphene in the Cu composite to investigate the role of the binder. All three different graphene derivatives show poor distribution in the Cu composites. This is mainly due to the weak interaction and different surface chemistry between graphene and Cu.[23] In order to increase the GRM-Cu interaction, the polymer-based binders (PVA and CNC) (Figure S4) were introduced (Scheme 1).

Owing to the binding effect of both CNC (Figures 1G–1I) and PVA (Figures 1J–1L), all three graphene derivatives show improved uniform distribution in the Cu matrix. However, the sample with CNC showed a higher propensity for particle agglomeration, possibly due to the hydrogen bonding inside the crystal during the drying,[24] as can be indicated in the SEM images in Figures 1H and 1I. The CNC crystals break into smaller particles covering the surface of the Cu, and leading to higher porosity and brittleness of the composite. However, the introduction of PVA leads to more uniform distribution of graphene in the Cu matrix (Figures 1I and 1J). According to the cross-sectional SEM images, one can observe that the PVA dispersed more uniformly between the Cu particles and the graphene, especially in the case of GO and RGO, compared with CNC (Figure S7). With such consideration, PVA was chosen as the binder for further investigation.

To further understand the distribution of graphene in Cu matrix, the pressed GO@PVA@Cu, RGO@PVA@Cu, and GNP@PVA@Cu samples were investigated by confocal Raman spectroscopy mapping. In agreement with the result obtained by SEM, the binary mixtures of Cu and GNP, GO, and RGO, respectively, show aggregation and poor distribution of graphene in the Cu matrix (Figures 2A, 2C, and 2E). In contrast, the addition of PVA significantly improved the uniformity of GNP, GO, and RGO in Cu matrix, as evidence by uniform color contrast indicated by the peak intensity of G band (Figures 2B, 2D, and 2F). The appearance of typical D band and G band in single spectra of corresponding samples confirmed the presence of different graphene derivatives, respectively (Figures 2G–2I). Both GO@PVA@Cu and RGO@PVA@Cu show an intense D band at 1350 cm^{-1} due to the presence of defects and oxygen containing groups on GO and RGO. The intensity ratio of the D band to G band (I_D/I_G) represents the defect ratio in the graphene. The Raman spectrum of GNP@PVA@Cu shows a weak D band and a strong G band with an I_D/I_G of 0.09, indicating low defect concentration and low level of oxidation. The I_D/I_G of RGO (1.38) is larger than that of GO (1.07) due to the reduction of GO.[25]

The optimal content of PVA to increase the homogeneous distribution of graphene derivatives in the Cu matrix was further investigated in pressed samples (Figure 3); the red arrow is used for marking the position of binder. Due to the different contrasts between C and Cu under SEM, the graphene derivatives (GNP, GO, and RGO) with different morphology in the Cu matrix can be identified. The distributed graphene embedded in Cu matrix shows the typical graphene morphology, which is consistent with the SEM images of pure graphene (Figure 1). As more PVA was added, the Cu powder tends to stick to nearby Cu particles. Moreover, as increasing the content of PVA binder, a slight

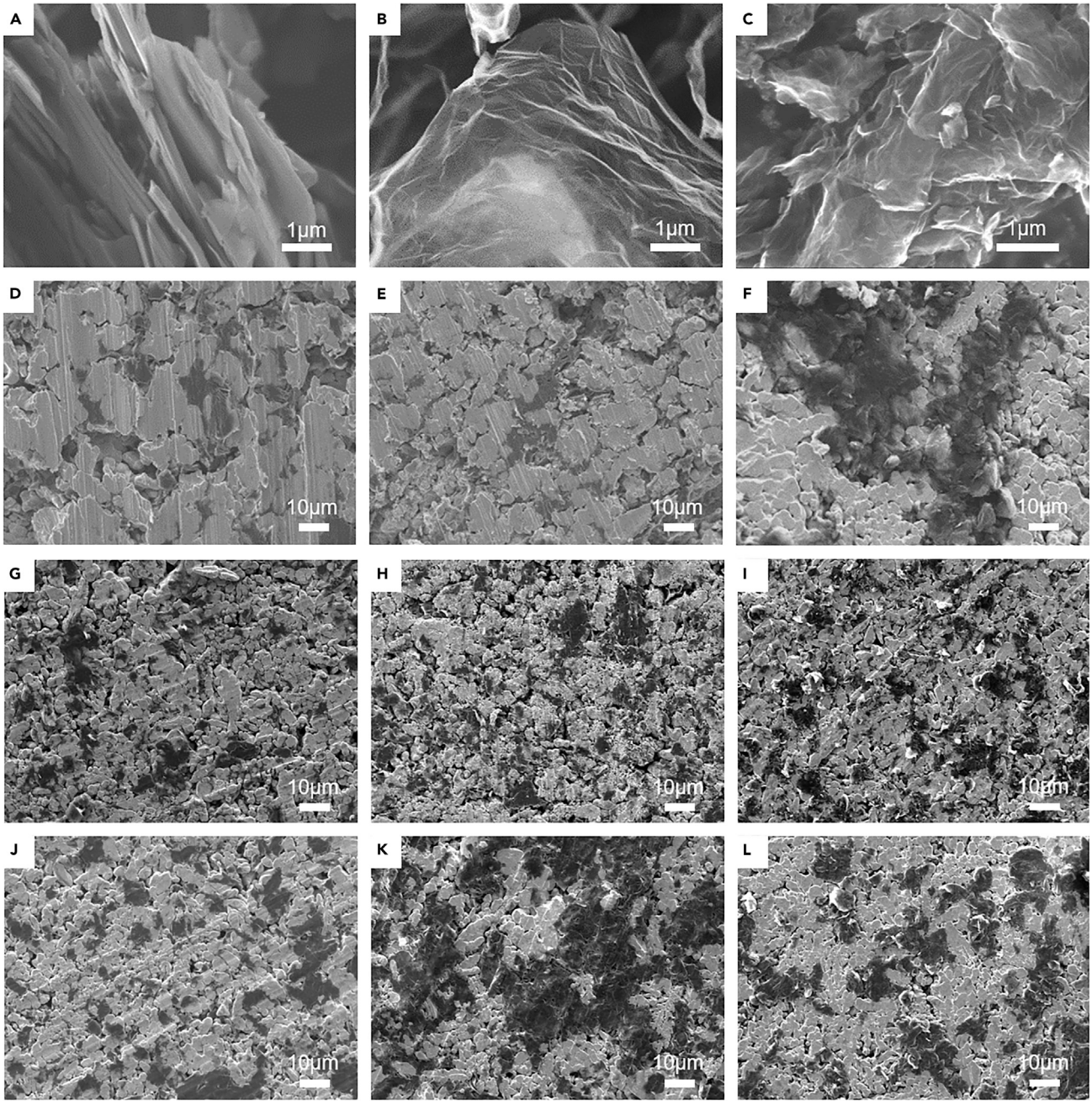

Figure 1. Effect of the binder on the morphology of the graphene derivatives containing Cu composites

SEM images of pure (A) GNP, (B) GO, (C) RGO; (D) pressed GNP(3%)/Cu, (E) GO(3%)/Cu, (F) RGO(3%)/Cu; (G) pressed GNP(3%)@CNC(2.8%)@Cu, (H) GO(3%)@CNC(2.8%)@Cu, (I)RGO(3%)@CNC (2.8%)@Cu; (J) pressed GNP(3%)@PVA(1.5%)@Cu, (K) GO(3%)@PVA(1.5%)@Cu, (L) RGO(3%)@PVA(1.5%)@Cu.

improvement of graphene distribution in Cu can also be observed in the case of GNP (Figures 3A and 3C). However, the incorporation of high content of PVA (2 wt %) leads to agglomeration of GO and RGO (Figure S8E and S8I), due to the strong interaction between oxygen groups on GO/RGO and the polar binder.[26–28] Moreover, the incorporation of a high content of PVA might bring potential problems, for example the formation of pores during sintering, caused by carbonization of PVA. In order to balance these impacts, the PVA content in the present study was set as 1 wt % when the graphene content was 3 wt %, which provided decent density and reduced porosity. Correspondingly, the contents of PVA were optimized as 0.5 wt % and 1.5 wt % when the graphene contents were 1 wt % and 5 wt %, respectively. Interestingly, the GO particles breaks into small particles and become partially exfoliated in GO@PVA@Cu sample, as we observed during the sample preparation.[29] As reported,[30] this was attributed to the diffusion of oxygen from the functional groups of GO into Cu, leading to the brittleness of

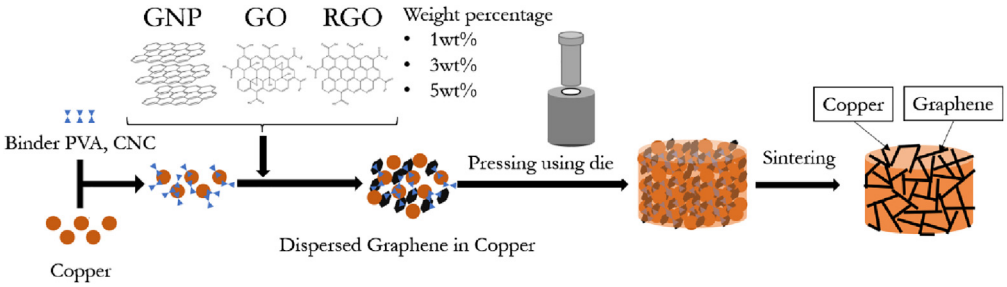

Scheme 1. Schematic illustration of the preparation of graphene@binder@Cu and sintering of graphene@binder@Cu

GO. In addition, SEM showed that also GNP@PVA@Cu and RGO@PVA@Cu composites had smaller particle size than the pristine GNP and RGO materials. This is because the mechanical mixing breaks the aggregated particles into smaller one. The smaller particles of graphene derivatives could positively affect their distribution in the Cu matrix and thus improve the tribological performance. The images with higher resolution are summarized in Figure S8.

To understand the thermal stability of graphene/Cu powder mixtures in the presence of binder, pure PVA, 5wt % GNP(GNP@PVA@Cu), 5wt % GO (GO@PVA@Cu), and 5wt % RGO (RGO@PVA@Cu) were analyzed by TGA (Figures 4A and 4B). Pure PVA shows major weight loss at ~300°C due to decomposition. This temperature is lower than the sintering temperature (above 900°C) of the Cu composite mixture, thus the binder can decompose (with the release of gas) during the composite sintering process. The weight loss of GNP(5%)@PVA(1.5%)@Cu and RGO(5%)@PVA(1.5%)@Cu at ~300°C is about 2% (note: the minor difference may be due to the absorbed water or the oxygen contenting functional groups from the GNP) and 1.5%, respectively, which is similar to the loading of PVA. However, the GO(5%)@PVA(1.5%)@Cu shows 2% weight loss at 200°C and additional 1% weight loss from 200 to 400°C, the former corresponding to the thermal decomposition of unstable oxygen-containing functional groups on GO,[31] and the latter is related to the decomposition of PVA and GO. Negligible weight loss at 200°C for GNP(5%)@PVA(1.5%)@Cu and RGO(5%)@PVA(1.5%)@Cu imply that both GNP and RGO have low oxygen content. During the thermal treatment of GO(5%)@PVA(1.5%)@Cu, the released gas (e.g., CO_2) cause the formation of pores in the sintered GO(5%)@PVA(1.5%)@Cu (Figure S9). With such consideration, the RGO is a better choice as starting materials than GO as lubricant additives in Cu.

The crystalline structures of the final mixed samples in comparison with pure Cu were also evaluated by XRD (Figures 4C and 4D). GNP(5%)@PVA(1.5%)@Cu, RGO(5%)@PVA(1.5%)@Cu, and GO(5%)@PVA(1.5%)@Cu all show the diffraction peaks of Cu at 43.28°, 50.40°, and 74.04°.

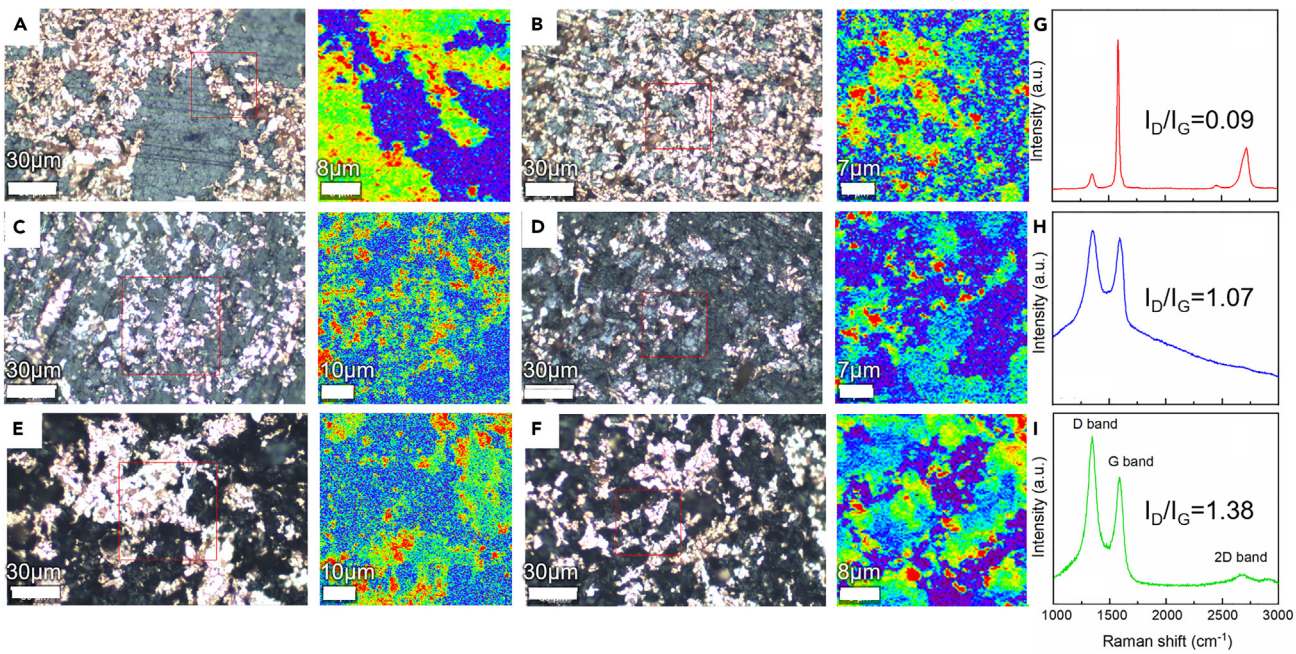

Figure 2. The distribution of the graphene derivatives in the Cu composites investigated by Raman

Raman mapping of pressed (A) GNP(3%)@Cu, (B) GNP(3%)@PVA(1.5%)@Cu, (C) GO(3%)@Cu, (D) GO(3%)@PVA(1.5%)@Cu, (E) RGO(3%)@Cu, (F) RGO(3%)@PVA(1.5%)@Cu and the corresponding single Raman spectrum shown in the right side of the figure (G–I).

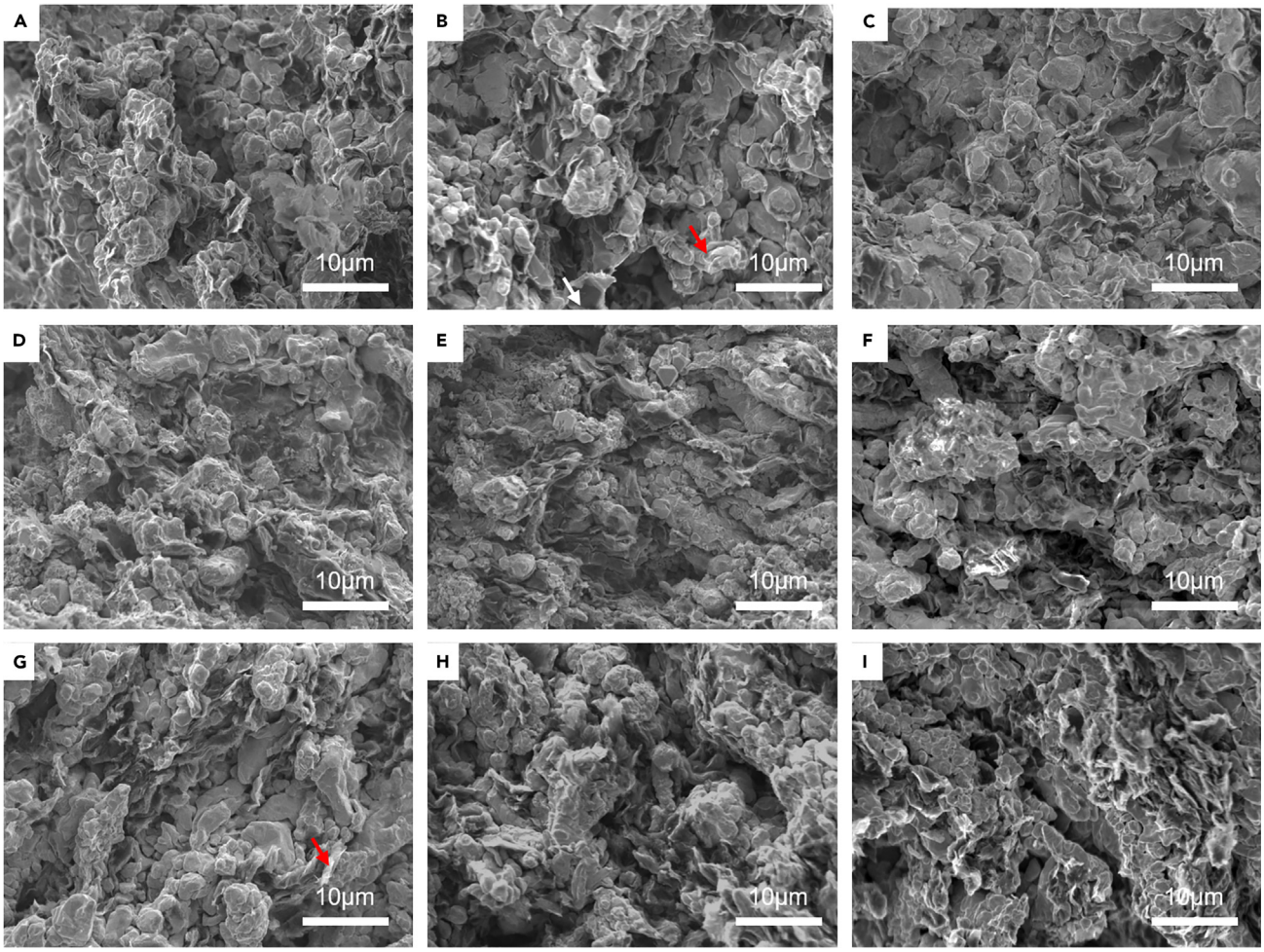

Figure 3. The effect of the PVA loading on the distribution of the graphene derivatives in Cu composites

SEM image of samples with three different ratios between graphene and PVA binder.

(A–C) GNP(3%)/Cu sample with 1%, 1.5% and 2% of PVA.

(D–F) GO(3%)/Cu sample with 1%, 1.5% and 2% of PVA.

(G–I) RGO(3%)/Cu sample with 1%, 1.5% and 2% of PVA.

The presence of a diffraction peak at 26° in the XRD spectrum of GNP(5%)@PVA(1.5%)@Cu confirmed the presence of the GNP, consisting of non-exfoliated multilayer graphene ([002] peak of graphite). However, no visible diffraction peak at 8–10° (GO[002] peak) or at 26° (RGO [002] peak) can be observed due to the low loading and uniform distribution of GO and RGO particles (Figure 4D).[32] Interestingly, Cu_2O diffraction peaks can be observed in the XRD pattern of GO(5%)@PVA(1.5%)@Cu, even in the simple powder mixtures. This was believed to be caused by the transfer of oxygen from the oxygen functional group on GO to Cu, resulting in the oxidation of Cu. The micrometer-sized Cu particles tend to be easily oxidized. This result further demonstrates that the GO may not be an ideal choice as starting material for Cu-graphene composites for tribology application.

The compressed GNP(5%)@PVA(1.5%)@Cu, RGO(5%)@PVA(1.5%)@Cu, and GO(5%)@PVA(1.5%)@Cu were sintered at 1025°C under Ar for 2 h. No significant structure change of the graphene component in the corresponding composites was observed after the sintering. The RGO(5%)@PVA(1.5%)@Cu and GO(5%)@PVA(1.5%)@Cu showed an optimal morphology under such conditions. The RGO after reduction is evenly distributed and embedded in the Cu matrix (Figures 5D–5F). However, under such sintering conditions, some of the Cu particles are not sintered in GNP(5%)@PVA(1.5%)@Cu (Figure S10), indicating the temperature might not be high enough to sinter Cu in the presence of GNP. This could be due to the good coverage of GNP on the Cu particles and large GNP flake size, preventing the Cu particles from sintering.

The sintering quality of GNP@PVA@Cu improved with increased sintering temperature from 1025°C to 1050°C (Figures 5A–5C). This might be due to the increased temperature resulting in faster diffusion of the Cu for the sintering. However, for GO@PVA@Cu and RGO@PVA@Cu samples melting occurs at 1050°C, especially at higher graphene content of 3 and 5 wt % (Figures S10D–S10I). This might be due to the high thermal conductivity of GO and RGO, resulting in improved heat transfer from graphene to Cu. The melted rod appears in the samples

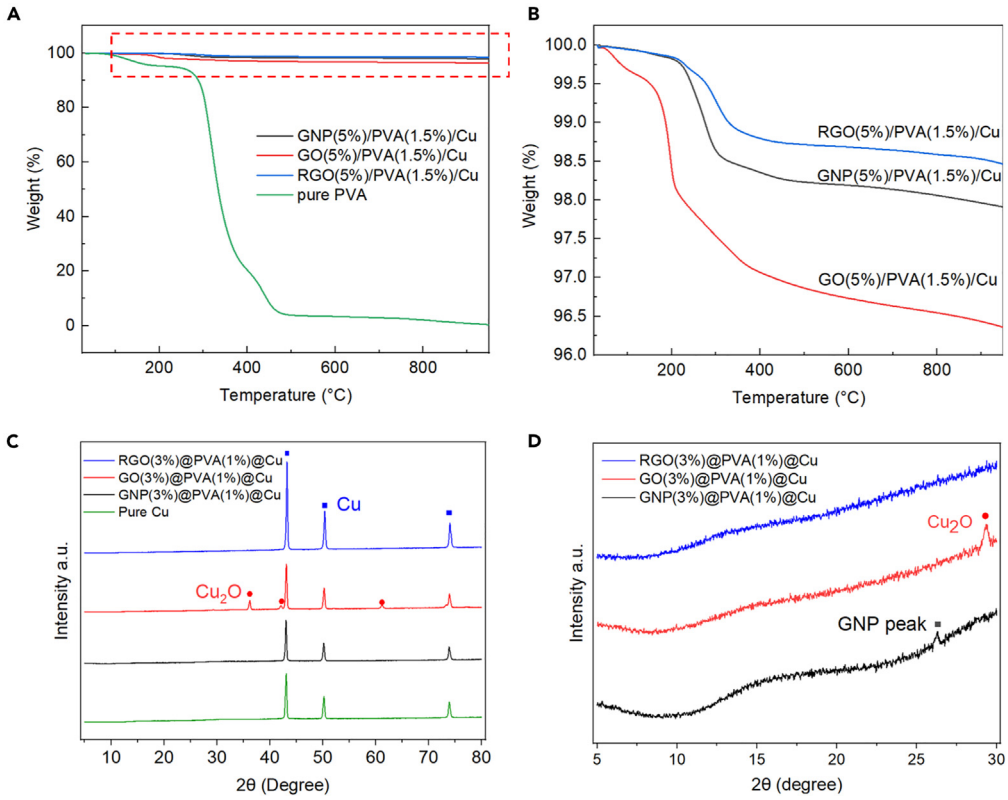

Figure 4. The thermal properties and structures of graphene derivatives containing Cu composites

(A) TGA of PVA, GNP(5%)@PVA(2%)@Cu, GO(5%)@PVA(2%)@Cu, and RGO(5%)@PVA(2%)@Cu powder mixtures; (B) zoom-in TGA curve of mixed samples; (C) XRD of pure Cu, GNP(3%)@PVA(1%)@Cu, GO(3%)@PVA(1%)@Cu, and RGO(3%)@PVA(1%)@Cu, (D) corresponding magnified XRD region from 5 to 30° in 2θ.

(Figure S10), because the sintering temperature is close to the melting temperature of Cu, which lead to the drastic change of morphology of sample even with increase of 25°C. Such structure will lead to lower hardness and the peeling off of graphene during the wear tests. The surface graphene also appears to vanish for some samples like 1wt % GO (Figure S10D). This may be attributed to the decomposition and subsequent depletion of GO due to the high oxygen content and high temperature.

In agreement with the fracture surface, metallurgical microscopic images of GNP@PVA@Cu, GO@PVA@Cu, and RGO@PVA@Cu also confirmed the homogeneously distributed graphene particles within the Cu matrix (Figure S11). Some pores can also be observed due to the improper compaction. However, the interface between graphene and Cu is clear, and no new phase can be observed, indicating that no reaction has been taken place during the sintering process. The SEM elemental mapping of GNP@PVA@Cu, GO@PVA@Cu, and RGO@PVA@Cu show the uniform distribution of the graphene derivatives in the Cu matrix (Figures S12–S14). As the loading of the graphene increase, the content of C element increases for all GNP@PVA@Cu, GO@PVA@Cu, and RGO@PVA@Cu samples.

For higher graphene derivatives loadings (5%), more graphene derivatives between the Cu particles and on the surface of compressed samples can be observed (Figures 5 and S10). However, the high loading could also cause agglomerations of graphene with poor distribution in the Cu matrix, especially for GO and RGO at 5 wt % (Figures 5F and 5I).

The electrical resistivity of the sintered composites lies in a range of about 200 mΩ (Figure S15). All samples are very conductive, similar to the pure Cu reference. The electrical conductivity of the pure GNP powder is higher than that of both pure GO and RGO powders. After the high temperature sintering, the GO and RGO component in the Cu composites have been completely reduced. Therefore, the resistivity of sintered GNP@PVA@Cu, GO@PVA@Cu, and RGO@PVA@Cu is in the same range. The resistivity of GNP@PVA@Cu shows negligible change after sintering. The density of the GNP@PVA@Cu, GO@PVA@Cu, and RGO@PVA@Cu is 7.05, 6.68, and 6.56 g/cm^3, which is lower than that of the pure Cu, due to the presence of the graphene and also the pores.

It is reported that 2D materials such as graphene, could achieve so called superlubricity,[33] and the incorporation of graphene into a metal matrix has been considered as a strategy to improve the tribological performance. Here, standard pin-on-disc reciprocal test was conducted to measure the frictional properties of the sintered Cu-graphene composites. The friction tests on all composites and reference pure Cu were performed at 3N or 10N load and 10mm stroke length, for a 200m travel distance in total, at an average speed of 5 cm/s (Figure 6). The counter surface used was chrome steel ball with 10mm diameter. For the sintered GO@PVA@Cu and RGO@PVA@Cu, the friction coefficient reduced at high graphene content of 5 wt %, as compare with the pure Cu (Figure S17). Although the sintered GO@PVA@Cu with 5wt % GO shows low friction coefficient, with an average of about 0.2, the curve is not very stable. The low friction is attributed to the uniform distribution of GO as

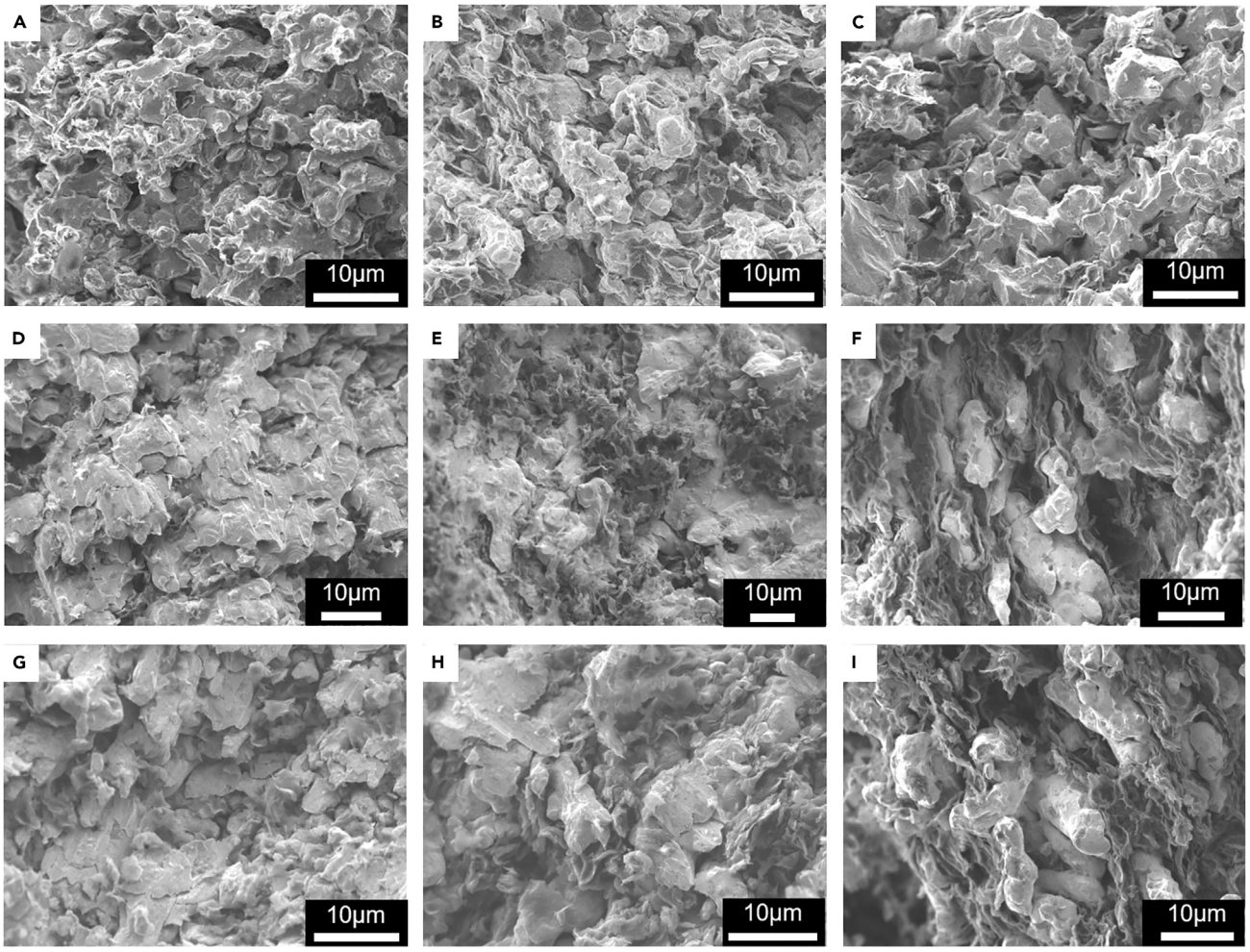

Figure 5. The morphology of the sintered graphene derivatives/binder/Cu composites

Fracture SEM images of (A–C) GNP@PVA@Cu with different graphene content (1%, 3%, and 5%), pressed and sintered at 1050°C for 1h; (D–F) GO@PVA@Cu with different graphene content (1%, 3%, and 5%), pressed and sintered at 1025°C for 1h.

(G–I) RGO@PVA@Cu with different graphene content (1%, 3%, and 5%), pressed and sintered at 1025°C for 1 h.

observed in SEM image, and the unstable performance could possibly be attributed to the presence of pores and the Cu_2O formed during the sintering process. A somewhat higher friction coefficient is observed for all RGO-containing samples. The reason is unclear at this point, but it might be due to poor distribution of RGO. In contrast to the RGO- and GO-containing samples, the sintered GNP@PVA@Cu samples all showed low friction coefficient (~0.2), even at 1wt % GNP loading. The stability improved with the increasing of GNP mass loading in the samples. The GNP composed by multilayer graphene act as an efficient lubricant under the friction force. The average friction coefficient of the GNP@PVA@graphene, GO@PVA@graphene, and RGO@PVA@graphene with three graphene loading (1 wt %, 3 wt %, and 5wt %) in comparison with Cu are summarized in Figures 6D–6F. In comparison, the friction test of the sintered GNP@PVA@Cu samples were performed under different loads (Figures S18 and S19). As the load increased from 3 N to 10 N, the average friction coefficient of both GNP (3%)@PVA(1%)@Cu and GNP (5%)@PVA(1.5%)@Cu slightly increased. However, the overall friction coefficient is still lower than 0.35.

In literature, it is discussed that the remaining oxygen-containing functional groups in GO and RGO acts as another medium for lubrication, and could contribute to lowering the friction. However, the accumulation of frictional heat in the local contact area leads to the oxidation, which prevent the dislocation created by the plastic deformation, and inducing high stress and great strain at the sub-surface,[34] leading to the increase and instability of coefficient of friction (CoF). In contrast, the CoF observed in GNP-containing samples are comparable to, and even more stable than, reported works.[35] The formation of graphene tribofilm in 5% of GNP sample is another important reason for the lower CoF, as can be confirmed in EDS (Figure S16). The wear rate is another indicator to the tribology performance. Simply by observing the depth of wear track and measuring the volume of the debris can one evaluate this property. Among all the samples, GO has the lowest wear rate, as it has the lowest amount of debris and the shallowest wear track. In addition, we also found that as more graphene derivatives (above 5 wt %)

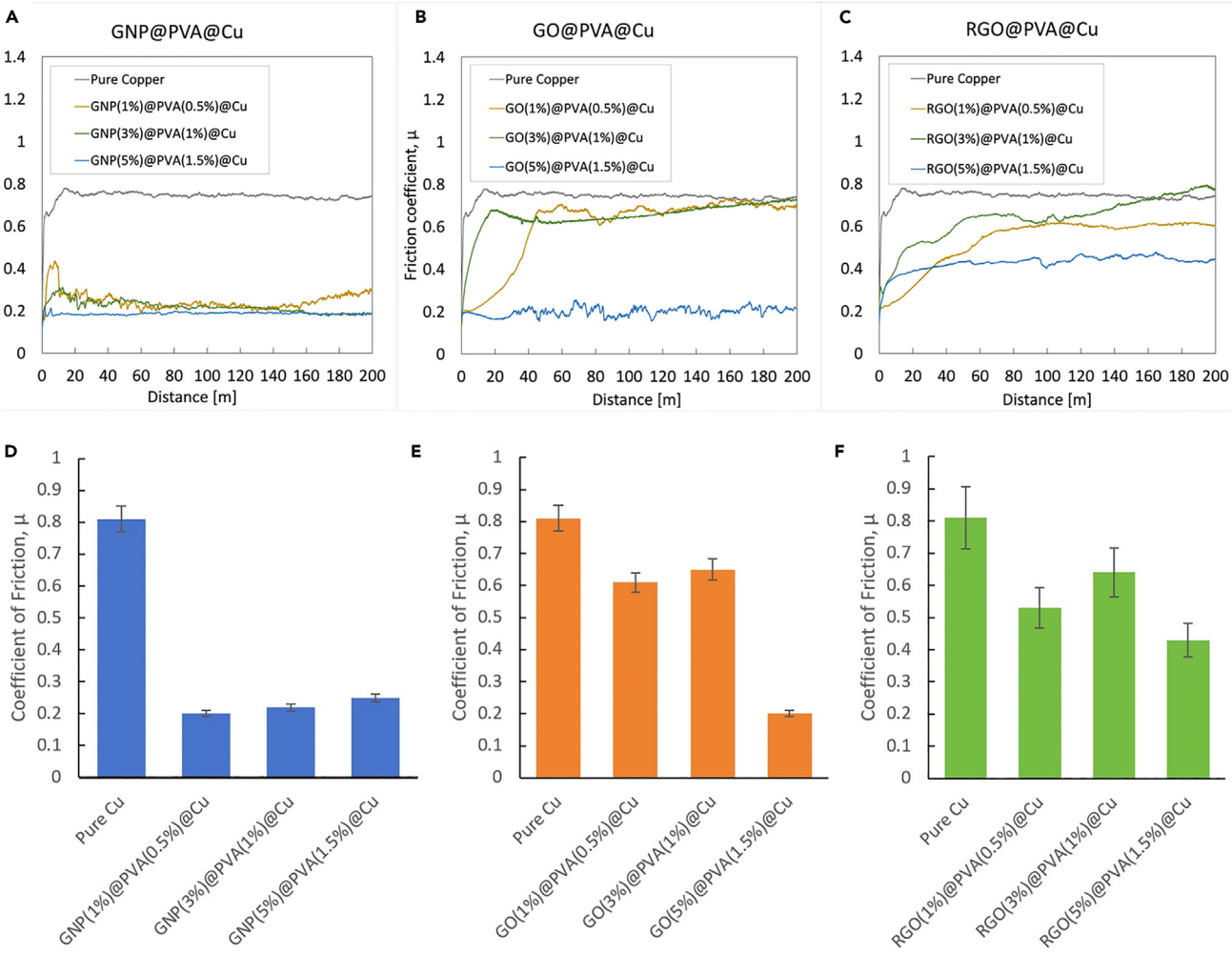

Figure 6. The tribological performance

The frictional coefficient vs. Distance graph of (A) sintered GNP@PVA@Cu with different graphene content from 1%, 3%, 5%; (B) sintered GO@PVA@Cu with different graphene content from 1%, 3%, 5%; (C) sintered RGO@PVA@Cu with different graphene content from 1%, 3%, 5%; all at 3N load. The average friction coefficient of (D) GNP@PVA@graphene, (E) GO@PVA@graphene, and (F) RGO@PVA@graphene with three graphene loading (1 wt %, 3 wt % and 5wt %) in comparison with Cu, showing the everage value.

added in the Cu composites, the sintered sample have poor wear resistance due to the presence of the large sized graphene particles in the Cu matrix leading to the poor sintering property.

SEM images showing the morphology and microstructures of worn surfaces are displayed in Figure 7. Spalling debris from the bulk materials and plowing microgrooves can be identified in sintered GNP(1%)@PVA(1%)@Cu sample after the wear test (Figures 7A and 7B). The debris is in the form of fine powder, with particle size around 1μm. Both abrasive and adhesive wear can be observed in this sample. When the GNP amount was increased to 3%, adhesive grooves (and a wider wear track) prevailed, and the grain appears. Smaller size of debris can be observed. Moreover, the GNP track is elongated along the sliding direction[36] (Figures 7C and 7D), forming the tribofilm. When the GNP content further increase to 5%, debris and microgrooves disappear, and the exposure of GNP can be clearly observed. This can be also confirmed by an increase in C content as measured by EDS (Figure S16). The exposure of GNP particles prevents the formation of oxide and leading to the low and stable friction coefficient.[35]

In order to further investigate the microstructure of different type of graphene containing samples after friction test, the 3N wear track morphologies of GNP(5%)@PVA(2%)@Cu, GO(5%)@PVA(2%)@Cu, and RGO(5%)@PVA(2%)@Cu were analyzed, as shown in Figure 8. There are severe plastic deformations and cracks, perpendicular to the sliding direction, in both GO@PVA@Cu and RGO@PVA@Cu samples. More debris are observed in GO@PVA@Cu sample, which is consistent with the previous result that the GO@PVA@Cu sample has lower binding strength. The mechanism leading to higher friction coefficient for RGO and less stable friction coefficient for GO might be that the crack impedes the lubrication effects of graphene, rather than the sliding of graphene. In contrast, the layer structure in GNP plays the critical role in

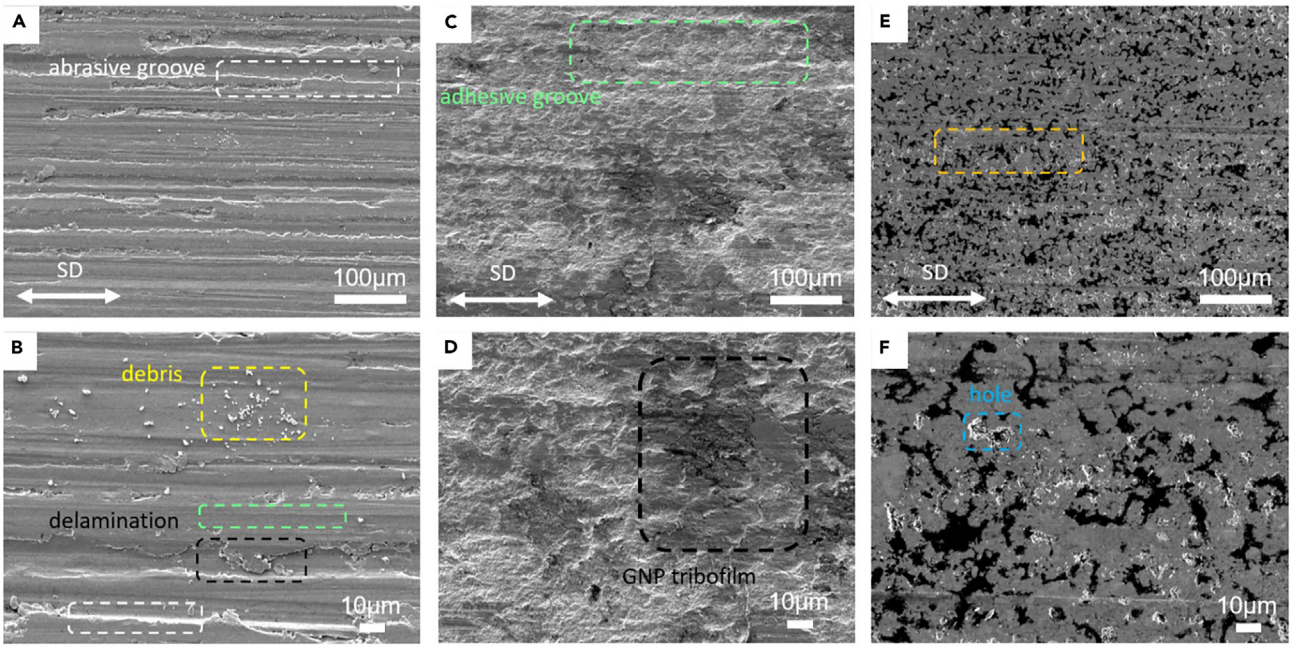

Figure 7. The wear track of sintered GNP@PVA@Cu with different binder loading

SEM images of the wear tracks of sintered GNP@PVA@Cu samples after tribological measurement under 3N load.
(A and B) sintered GNP(1%)@PVA(0.5%)@Cu, (C and D) GNP(3%)@PVA(1%)@Cu, (E and F) sintered GNP(5%)@PVA(1.5%)@Cu.

the lubrication effect, because it can easily slide to each other, whereas the defects (functional group in both surface and edge) in GO and RGO further decrease the lubrication property. During wear test, the GO or RGO forms GO-adsorption film and a tribochemical film which prevent the direct contact between the frictional object (the Cu matrix and the friction ball).[37] The effect is minimized in GNP containing samples, and thus it shows the equivalent superlubricity as the surface lubricated by oil.[38]

Conclusions

In this work, we investigated and evaluated the tribological performance of three different commercialized graphene derivatives (e.g., GO, RGO, and GNP) as additives in Cu matrix composites. To increase the interaction of graphene derivatives with Cu particles and while addressing the aggregation problem of graphene, different binders (PVA, CNC) were introduced into the system. The water soluble PVA shows better binding function than CNC. The graphene derivatives benefit from the addition of PVA, and are evenly distributed in the Cu matrix even at a high graphene loading of up to 5 wt %. After sintering at 1025 or 1050°C, the graphene was preserved and well distributed in the Cu as determined by SEM, EDS, and Raman mapping. The tribological performance shows that the GNP(3%)@PVA(2%)@Cu sample sintered at 1050°C for 1.5h has the lowest coefficient of friction and outperforms the GO and RGO containing samples. With this, the tribological properties of graphene derivatives are better understood and it could be demonstrated that the combination of graphene derivatives and binder is promising for industrial application.

Limitation of the study

Further work needs to be done to measure the wear rate of the graphene containing sample to understand the anti-wear performance of the sample. In addition, some advanced characterization for example perform the friction test under different conditions (different humidity and temperature).

STAR★METHODS

Detailed methods are provided in the online version of this paper and include the following:

- KEY RESOURCES TABLE
- RESOURCE AVAILABILITY
  - Lead contact
  - Materials availability
  - Data and code availability
- EXPERIMENTAL MODAL AND STUDY PARTICIPANT DETAILS

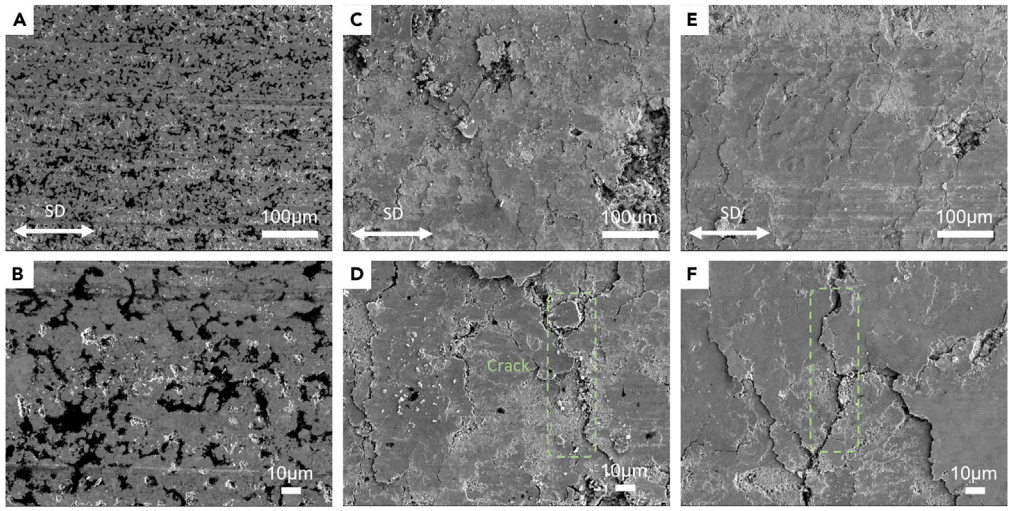

Figure 8. The effect of the different graphene derivatives on the wear track of sintered composites

The SEM image of wear tracks from 5% sample, (A and B) GNP(5%)@PVA(2%)@Cu, (C and D) GO(5%)@PVA(2%)@Cu, (E and F) RGO(5%)@PVA(2%)@Cu, all at 3N load.

SUPPLEMENTAL INFORMATION

Supplemental information can be found online at https://doi.org/10.1016/j.isci.2024.109429.

ACKNOWLEDGMENTS

The research leading to these results was funded by European Union's Horizon 2020 research and innovation program in GrapheneCore3 881603–Graphene Flagship (Spearhead 3 project and WP14), the Swedish Research Council in project Janus 2017-04456, FLAG-ERA project (2019-03411 and 2021-05924), the ÅForsk Young Researcher project (21–393), VINNOVA project (2021-05121) and 2D TECHVINNOVA competence Center (2019–00068). This work was performed, in part, at Chalmers Materials Analysis Laboratory.

AUTHOR CONTRIBUTIONS

J.S. conceived the study; C.H. synthesized the materials and performed the characterizations; S.Z., E.J., and A.M.A., performed the friction test and data analysis; All authors discussed, wrote, and commented on the manuscript.

DECLARATION OF INTERESTS

The authors declare no competing interests.

Received: October 22, 2023
Revised: January 9, 2024
Accepted: March 4, 2024
Published: March 6, 2024

REFERENCES

1. Sun, J., and Du, S. (2019). Application of graphene derivatives and their nanocomposites in tribology and lubrication: a review. RSC Adv. *9*, 40642–40661.
2. Liu, H., Xie, M., Pan, B., Li, N., Zhang, J., Lu, M., Luo, J., and Wang, H. (2022). In-situ intercalated pyrolytic graphene/serpentine hybrid as an efficient lubricant additive in paraffin oil. Colloid. Surface. *652*, 129929. https://doi.org/10.1016/j.colsurfa.2022.129929.
3. Liu, H., Xie, M., Pan, B., Wang, B., Zhang, L., Zhou, Y., Li, N., Yue, E., and Wang, H. (2023). Boosting the tribological properties of PEG200 by a novel face-to-face FeOCl/Zn-MOF lubricant additive. J. Mol. Liq. *391*, 123409.
4. Spear, J.C., Ewers, B.W., and Batteas, J.D. (2015). 2D-nanomaterials for controlling friction and wear at interfaces. Nano Today *10*, 301–314. https://doi.org/10.1016/j.nantod.2015.04.003.

5. Berman, D., Erdemir, A., and Sumant, A.V. (2014). Graphene: a new emerging lubricant. Mater. Today *17*, 31–42. https://doi.org/10.1016/j.mattod.2013.12.003.
6. Kim, K.S., Lee, H.J., Lee, C., Lee, S.K., Jang, H., Ahn, J.H., Kim, J.H., and Lee, H.J. (2011). Chemical Vapor Deposition-Grown Graphene: The Thinnest Solid Lubricant. ACS Nano *5*, 5107–5114. https://doi.org/10.1021/nn2011865.
7. Sun, J., Hwang, J.Y., Jankowski, P., Xiao, L., Sanchez, J.S., Xia, Z., Lee, S., Talyzin, A.V., Matic, A., Palermo, V., et al. (2021). Critical Role of Functional Groups Containing N, S, and O on Graphene Surface for Stable and Fast Charging Li-S Batteries. Small *17*, e2007242. https://doi.org/10.1002/smll.202007242.
8. Sun, Y., Sun, J., Sanchez, J.S., Xia, Z., Xiao, L., Chen, R., and Palermo, V. (2023). Surface chemistry and structure manipulation of graphene-related materials to address the challenges of electrochemical energy storage. Chem. Commun. *59*, 2571–2583. https://doi.org/10.1039/d2cc06772b.
9. Kovtun, A., Treossi, E., Mirotta, N., Scidà, A., Liscio, A., Christian, M., Valorosi, F., Boschi, A., Young, R.J., Galiotis, C., et al. (2019). Benchmarking of graphene-based materials: real commercial products versus ideal graphene. 2D Mater. *6*, 025006. https://doi.org/10.1088/2053-1583/aafc6e.
10. Sun, J., Klechikov, A., Moise, C., Prodana, M., Enachescu, M., and Talyzin, A.V. (2018). A Molecular Pillar Approach To Grow Vertical Covalent Organic Framework Nanosheets on Graphene: Hybrid Materials for Energy Storage. Angew Chem Int Edit *57*, 1034–1038. https://doi.org/10.1002/anie.201710502.
11. Sun, J., Memon, M.A., Bai, W., Xiao, L., Zhang, B., Jin, Y., Huang, Y., and Geng, J. (2015). Controllable Fabrication of Transparent Macroporous Graphene Thin Films and Versatile Applications as a Conducting Platform. Adv. Funct. Mater. *25*, 4334–4343. https://doi.org/10.1002/adfm.201501733.
12. Hidalgo-Manrique, P., Lei, X., Xu, R., Zhou, M., Kinloch, I.A., and Young, R.J. (2019). Copper/graphene composites: a review. J. Mater. Sci. *54*, 12236–12289.
13. Zhou, J., Wang, Q., Sun, Q., Chen, X.S., Kawazoe, Y., and Jena, P. (2009). Ferromagnetism in semihydrogenated graphene sheet. Nano Lett. *9*, 3867–3870.
14. Sun, J., Sadd, M., Edenborg, P., Grönbeck, H., Thiesen, P.H., Xia, Z., Quintano, V., Qiu, R., Matic, A., and Palermo, V. (2021). Real-time imaging of Na+ reversible intercalation in "Janus" graphene stacks for battery applications. Sci. Adv. *7*, eabf0812. https://doi.org/10.1126/sciadv.abf0812.
15. Sun, J., Martinsen, K.H., Klement, U., Kovtun, A., Xia, Z., Silva, P.F.B., Hryha, E., Nyborg, L., and Palermo, V. (2023). Controllable Coating Graphene Oxide and Silanes on Cu Particles as Dual Protection for Anticorrosion. ACS Appl. Mater. Interfaces *15*, 38857–38866. https://doi.org/10.1021/acsami.3c08042.
16. Chu, K., and Jia, C. (2014). Enhanced strength in bulk graphene–copper composites. physica status solidi (a) *211*, 184–190. https://doi.org/10.1002/pssa.201330051.
17. Ayyappadas, C., Muthuchamy, A., Raja Annamalai, A., and Agrawal, D.K. (2017). An investigation on the effect of sintering mode on various properties of copper-graphene metal matrix composite. Adv. Powder Technol. *28*, 1760–1768. https://doi.org/10.1016/j.apt.2017.04.013.
18. Li, J.T., Wu, Z.Y., Lu, Y.Q., Zhou, Y., Huang, Q.S., Huang, L., and Sun, S.G. (2017). Water soluble binder, an electrochemical performance booster for electrode materials with high energy density. Adv. Energy Mater. *7*, 1701185.
19. Park, H.-K., Kong, B.-S., and Oh, E.-S. (2011). Effect of high adhesive polyvinyl alcohol binder on the anodes of lithium ion batteries. Electrochem. Commun. *13*, 1051–1053.
20. Song, J., Zhou, M., Yi, R., Xu, T., Gordin, M.L., Tang, D., Yu, Z., Regula, M., and Wang, D. (2014). Interpenetrated gel polymer binder for high-performance silicon anodes in lithium-ion batteries. Adv. Funct. Mater. *24*, 5904–5910.
21. Jiang, L., Fan, G., Li, Z., Kai, X., Zhang, D., Chen, Z., Humphries, S., Heness, G., and Yeung, W.Y. (2011). An approach to the uniform dispersion of a high volume fraction of carbon nanotubes in aluminum powder. Carbon *49*, 1965–1971.
22. Sun, J., Iakunkov, A., Rebrikova, A.T., and Talyzin, A.V. (2018). Exactly matched pore size for the intercalation of electrolyte ions determined using the tunable swelling of graphite oxide in supercapacitor electrodes. Nanoscale *10*, 21386–21395. https://doi.org/10.1039/c8nr07469k.
23. Hidalgo-Manrique, P., Lei, X., Xu, R., Zhou, M., Kinloch, I.A., and Young, R.J. (2019). Copper/graphene composites: a review. J. Mater. Sci. *54*, 12236–12289. https://doi.org/10.1007/s10853-019-03703-5.
24. Sinquefield, S., Ciesielski, P.N., Li, K., Gardner, D.J., and Ozcan, S. (2020). Nanocellulose dewatering and drying: current state and future perspectives. ACS Sustain. Chem. Eng. *8*, 9601–9615.
25. Scardaci, V., and Compagnini, G. (2021). Raman Spectroscopy Investigation of Graphene Oxide Reduction by Laser Scribing. Chimia *7*, 48.
26. Morimune, S., Nishino, T., and Goto, T. (2012). Poly(vinyl alcohol)/graphene oxide nanocomposites prepared by a simple eco-process. Polym. J. (Tokyo, Jpn.) *44*, 1056–1063. https://doi.org/10.1038/pj.2012.58.
27. Manna, K., Srivastava, S.K., and Mittal, V. (2016). Role of Enhanced Hydrogen Bonding of Selectively Reduced Graphite Oxide in Fabrication of Poly(vinyl alcohol) Nanocomposites in Water as EMI Shielding. J. Phys. Chem. C *120*, 17011–17023. https://doi.org/10.1021/acs.jpcc.6b03356.
28. De, S., Purcell, C., Murley, J., Flouda, P., Shah, S., Green, M., and Lutkenhaus, J. (2018). Spray-On Reduced Graphene Oxide-Poly(vinyl alcohol) Supercapacitors for Flexible Energy and Power. Adv. Mater. Interfaces *5*, 1801237. https://doi.org/10.1002/admi.201801237.
29. Jiang, R., Zhou, X., Fang, Q., and Liu, Z. (2016). Copper–graphene bulk composites with homogeneous graphene dispersion and enhanced mechanical properties. Materials Science and Engineering: A *654*, 124–130.
30. Nautiyal, H., Kumari, S., Rao, U.S., Tyagi, R., and Khatri, O.P. (2020). Tribological Performance of Cu-rGO-MoS2 Nanocomposites Under Dry Sliding. Tribol. Lett. *68*, *29*. https://doi.org/10.1007/s11249-020-1270-8.
31. Alam, S.N., Sharma, N., and Kumar, L. (2017). Synthesis of graphene oxide (GO) by modified hummers method and its thermal reduction to obtain reduced graphene oxide (rGO). Graphene *06*, 1–18.
32. Sun, J.H., Morales-Lara, F., Klechikov, A., Talyzin, A.V., Baburin, I.A., Seifert, G., Cardano, F., Baldrighi, M., Frasconi, M., and Giordani, S. (2017). Porous graphite oxide pillared with tetrapod-shaped molecules. Carbon *120*, 145–156. https://doi.org/10.1016/j.carbon.2017.05.007.
33. Berman, D., Erdemir, A., and Sumant, A.V. (2018). Approaches for Achieving Superlubricity in Two-Dimensional Materials. ACS Nano *12*, 2122–2137. https://doi.org/10.1021/acsnano.7b09046.
34. Qiang, Y., Ge, S., and Xue, Q. (1999). Microstructure and tribological behaviour of nitrocarburizing-quenching duplex treated steel. Tribol. Int. *32*, 131–136.
35. Chen, F., Ying, J., Wang, Y., Du, S., Liu, Z., and Huang, Q. (2016). Effects of graphene content on the microstructure and properties of copper matrix composites. Carbon *96*, 836–842.
36. Lian, W., Mai, Y., Wang, J., Zhang, L., Liu, C., and Jie, X. (2019). Fabrication of graphene oxide-Ti3AlC2 synergistically reinforced copper matrix composites with enhanced tribological performance. Ceram. Int. *45*, 18592–18598. https://doi.org/10.1016/j.ceramint.2019.06.082.
37. Wu, L., Xie, Z., Gu, L., Song, B., and Wang, L. (2018). Investigation of the tribological behavior of graphene oxide nanoplates as lubricant additives for ceramic/steel contact. Tribol. Int. *128*, 113–120.
38. Ge, X., Li, J., Luo, R., Zhang, C., and Luo, J. (2018). Macroscale Superlubricity Enabled by the Synergy Effect of Graphene-Oxide Nanoflakes and Ethanediol. ACS Appl. Mater. Interfaces *10*, 40863–40870. https://doi.org/10.1021/acsami.8b14791.

STAR★METHODS

KEY RESOURCES TABLE

REAGENT or RESOURCE	SOURCE	IDENTIFIER
Chemicals, peptides, and recombinant proteins		
Copper powder	Kebo AB Stockholm	CAS: 7440-50-8
Polyvinyl Alcohol	Sigma Aldrich	CAS: 9002-89-5
Cellulose NanoCrystals	Celluforce	CAS: 9004-34-6
GNP	Graphmatech AB	https://graphmatech.com/
GO	LayerOne	https://www.layeronematerials.com/
RGO	Graphmatech AB	https://graphmatech.com/

RESOURCE AVAILABILITY

Lead contact

Further information and other requests should be directed to and will be fulfilled by the lead contact, Jinhua Sun (jinhua@chalmers.se).

Materials availability

This work did not generate new unique reagents.

Data and code availability

- All data reported in this paper will be shared by the lead contact upon request.
- This paper does not report original code.
- Any additional information required to reanalyze the data reported in this paper is available from the lead contact upon request.

EXPERIMENTAL MODAL AND STUDY PARTICIPANT DETAILS

This work did not include any experimental model or study participants.

METHOD DETAILS

Synthesis of graphene/Cu and graphene/binder/Cu composites

To prepare the graphene/binder/Cu composite mixtures, the binder (PVA or CNC) was firstly dissolved in the water, and then mixed with copper particles in different ratios (from 1 to 3 wt%) using a mortar and pestle, followed by adding different graphene derivatives (Scheme 1). The mixtures were mechanically mixed until a uniform paste was obtained. The mixture was then vacuum dried at room temperature for 12h. For the different graphene/Cu composites mixtures, the same procedure was followed, just excluding the addition of the binder. A H100 hydraulic press with die was used to press the samples into disk-shaped platelets. Ca. 1g as-prepared composite mixture was pressed under a pressure of 5584 MPa. The compressed samples (green bodies) were sintered in a tube furnace at 1025°C or 1050°C at 5°C/min heating rate for one hour under Ar. After cooling to room temperature, the sintered samples were obtained for further characterizations.

Characterization

A JEOL JSM-7800F Prime scanning electron microscope (SEM) equipped with energy-dispersive X-ray spectroscopy (EDS) was used to analyze the morphology, porosity, and the distribution of graphene in the copper matrix. Raman analysis was performed using a WITec alpha300 R (532 nm laser) spectrometer operating at low power. The aim was to confirm the existence and distribution of graphene after sintering. X-ray Diffraction (XRD) (Bruker Discover D8) was used to characterize the graphene/Cu samples. Hardness (HV5) was measured with a Struers DuraScan. Five measurements at an interval of 2 mm were taken for each sample, and the average hardness were then calculated. Resistivity was measured using a standard four-point probe (2450 SourceMeter Keithley). Thermogravimetric analysis (TGA) (TGA/DSC 3+) was used to understand the thermal stability of the samples under Ar, and 5°C/min heating rate was used for all samples. The equipment used for the tribology test is CSM Tribometer. The friction tests on all composites and reference pure Cu were performed at 3N or 10 N load and 10mm stroke length, for a 200m travel distance in total, at an average speed of 5 cm/s. The counter surface is chrome steel ball (AISI 52100 UNI 100C6) with diameter of 10 mm. The tribology test was performed under room

temperature and ambient conditions (humidity: ca. 70%). The friction test was carried out at 3N, corresponding to 664 MPa Hertzian contact pressure.

QUANTIFICATION AND STATISTICAL ANALYSIS

This article does not include statistical analysis.